Pure appl. geophys. 165 (2008) 1249–1262
0033–4553/08/071249–14
DOI 10.1007/s00024-008-0355-3

Pure and Applied Geophysics

Receiver Functions for Three-layer Media

CHI-CHIA TANG,[1] CHAU-HUEI CHEN,[1,*] and TA-LIANG TENG[2]

Abstract—We have extended the H-k stacking method of receiver functions applicable to a three-layer model, which is useful in studying detailed crustal structures. We have demonstrated its application with two sample sites in Taiwan, making use of travel times of converted phases from the direct P waves of teleseismic events as the P reflects and refracts at different discontinuities in the crust. This three-layer extension allows a closer examination on the crust, as well as the relationship between crustal layers and the associated V_p/V_s ratios. Data were processed using the multiple-taper correlation technique to obtain the radial receiver functions (RRFs). The relative time delays of the converted phases measured from the RRFs were used to estimate the depths of the crustal discontinuities. Results not only yield the depths to principal crustal layers, including the Moho, but also give the corresponding ranges of V_p/V_s ratio which are comparable with findings from other tomographic studies.

Key words: Receiver function, three-layer media.

1. Introduction

Since the first paper by PHINNEY (1964), teleseismic body waves are often used to investigate the structure of crust. In recent years, the method of receiver function has been successfully applied to studies of the structure of the crust, especially to the estimation of the Moho depth. Among others, receiver functions are used to map the Moho depth in several areas around the world (ZHU and KANAMORI, 2000; LEVIN *et al.*, 2002; PARK and LEVIN, 2000; LEVIN and PARK, 1997a, b, 1998, 2000; OWENS and CROSSON, 1988, to name a few). However, these studies mostly focused on estimating only the crustal thickness. There have been comparatively few studies devoted to a layered crustal structure. In this study, we noticed the complexities generally involved in the direct P waves that give rise to clear multiple phases on the radial receiver functions (RRFs) profiles. We then have extended the stacking method which was developed by ZHU and KANAMORI (2000) to a three-layer crustal model for the delineation of a layered crustal structure as well as the Moho depth. This is essentially an interpretation of multiple P-S converted phases which

[1] Institute of Seismology, National Chung Cheng University, 168, University Rd., Min-Hsiung Chia-Yi, Taiwan, R.O.C. E-mail: seichen@eq.ccu.edu.tw

[2] Dept. of Earth Sciences, Univ. Southern California, Zumberge Hall, University of Southern California 3651 Trousdale Parkway, Los Angeles, CA 90089, USA

* Corresponding author.

are refracted and reflected at different discontinuities in the crust. In order to clearly identify these multiple converted phases against a normally noisy background, stacking of numerous radial receiver functions allows a significant improvement of the signal-to-noise ratio, and consequently a clearer extraction of crustal layering information is possible.

2. Method

ZHU and KANAMORI (2000) developed a stacking algorithm that used the amplitudes of teleseismic multiple P-S converted phases and differential times between direct P and other P-S converted phases to calculate the Moho depth and V_p/V_s ratios beneath the station. They have successfully applied this stacking algorithm to obtaining Moho depths and V_p/V_s ratios of Southern California. For a single-layer crustal model, there are three converted phase on the RRFs profile. The corresponding ray paths of these converted phases have been shown in Figure 1a. The synthetic RRFs for a laterally homogeneous and isotropic single-layer model is shown as Figure 1b with different ray parameter. Relations between the depth of Moho discontinuity (H_{Moho}) and the crustal V_p/V_s ratio (k_m) for this model can be written as follows (ZHU and KANAMORI, 2000), noting that $1/V_s^2 = k_m^2/V_p^2$

$$H_{Moho} = \frac{t_{Ps}}{\sqrt{\frac{k_m^2}{V_p^2} - p^2} - \sqrt{\frac{1}{V_p^2} - p^2}} \tag{1}$$

$$H_{Moho} = \frac{t_{PpPs}}{\sqrt{\frac{k_m^2}{V_p^2} - p^2} + \sqrt{\frac{1}{V_p^2} - p^2}} \tag{2}$$

$$H_{Moho} = \frac{t_{PpSs+PsPs}}{2\sqrt{\frac{k_m^2}{V_p^2} - p^2}}, \tag{3}$$

where t_{Ps} is the differential travel-time between the direct P wave and the Ps phase; t_{PpPs} is the differential travel-time between direct P and PpPs, and $t_{PpSs\ +\ PsPs}$ is the differential time between direct P and PpSs + PsPs. V_p and V_s represent the P-wave and S-wave velocities, respectively; and *p* is the ray parameter. From equations (1)–(3), we can use the H-k stacking method developed by ZHU and KANAMORI (2000) to estimate the Moho depth. Here, stacking is necessary as the Moho and crustal discontinuities are clearly not strictly planar.

This paper extends the single-layer to a three-layer crustal model for more careful delineation of discontinuities existing in the crust. To demonstrate our method, we begin with a three-layer crust above the Moho shown in Figure 1c. For a three-layer crustal model, the incident P waves will generate mutiple P-S converted waves which resulted

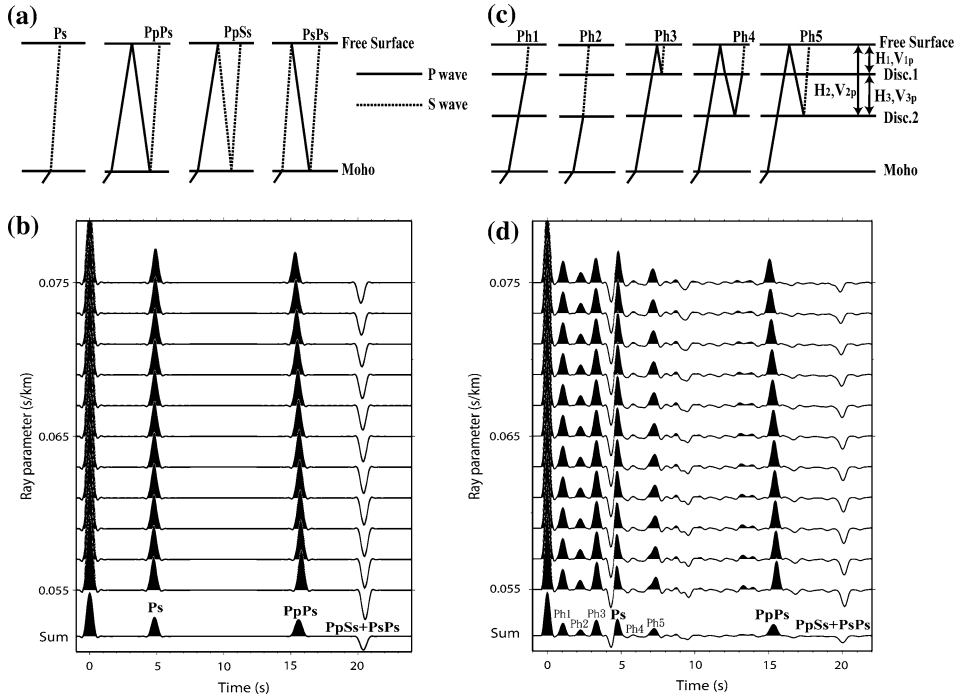

Figure 1

(a)–(b) The ray paths of P-S converted phases for a single-layer and a three-layer media. The solid line indicates P-wave ray path and the dashed line indicates S-wave ray path. V_{1p} and H_1 express the average P-wave velocity and the thickness between discontinuity 1 and the free surface; the V_{2p} and H_2 express the average P-wave velocity and the thickness between discontinuity 2 and the free surface; and the V_{3p} and H_3 express the average P-wave velocity and the thickness between discontinuities 1 and 2. Five identifiable converted phases in a three-layer medium are marked by Ph1 through Ph5. **(c)** and **(d)** give synthetic RRF profiles, and corresponding phases for a single-layer and a three-layer media are shown with different ray parameters.

from reflection and refraction at these layer boundaries. The corresponding ray paths are shown in Figure 1c. For different ray parameter p, a synthetic RRFs profile for a laterally homogeneous and isotropic three-layer crustal model is shown in Figure 1d drawn for a reference model (Table 1). Five strongest converted phases are labeled with Ph1 through Ph5 by their arrival times on RRFs profile and can also be estimated from the reference crustal velocity model.

Ph1 is a P-S converted phase from discontinuity 1 and Ph3 is a multiple phase of Ph1. These two phases have comparable amplitudes. Similarly, Ph2 is a P-S converted phase from discontinuity 2 and Ph5 is a multiple phase of Ph2. Ph4 is a P-SV conversion at discontinuity 1 after the direct P wave reflects first at the free surface and at discontinuity 2. With these definitions, we have extended (1) and (2) to two sets of equations involving H_1 and H_2 shown in Figure 1c:

Table 1

The Reference Velocity Model (CHEN et al., 1994)

Layer	Thickness, km	V_p, km/s	V_p/V_s
1	6	5.0	1.85
2	9	6.0	1.8
3	20	6.5	1.78
4	-	8.0	1.78

$$H_1 = \frac{t_{Ph1}}{\sqrt{\frac{k_1^2}{V_{1p}^2} - p^2} - \sqrt{\frac{1}{V_{1p}^2} - p^2}}, \tag{4}$$

$$H_1 = \frac{t_{Ph3}}{\sqrt{\frac{k_1^2}{V_{1p}^2} - p^2} + \sqrt{\frac{1}{V_{1p}^2} - p^2}}, \tag{5}$$

where t_{Ph1} is the travel-time difference between Ph1 and the direct P wave and t_{Ph3} is the travel-time difference between Ph3 and the direct P wave, and k_1 is the V_p/V_s ratio between discontinuity 1 and the free surface.

We can estimate the H_2 by a similar manner giving a second set of these equations as:

$$H_2 = \frac{t_{Ph2}}{\sqrt{\frac{k_2^2}{V_{2p}^2} - p^2} - \sqrt{\frac{1}{V_{2p}^2} - p^2}} \tag{6}$$

$$H_2 = \frac{t_{Ph5}}{\sqrt{\frac{k_2^2}{V_{2p}^2} - p^2} + \sqrt{\frac{1}{V_{2p}^2} - p^2}}, \tag{7}$$

where t_{Ph2} is the travel-time difference between Ph2 and the direct P wave and t_{Ph5} is the travel-time difference between Ph5 and the direct P wave and k_2 is the V_p/V_s ratio between discontinuity 2 and the free surface.

In a grid-search method similar to that used by ZHU and KANAMORI (2000), we define S_1 and S_2 as

$$S_1(H_1, k_1) = w_{Ph1} r(t_{Ph1}) + w_{Ph3} r(t_{Ph3}) \tag{8}$$

$$S_2(H_2, k_2) = w_{Ph2} r(t_{Ph2}) + w_{Ph5} r(t_{Ph5}), \tag{9}$$

where r(t) is the corresponding RRF, and t_{Ph1}, t_{Ph2}, t_{Ph3}, and t_{Ph5} are the predicted Ph1, Ph2, Ph3, and Ph5 arrival times. w_{Phi} is the weighting factor for the Phi phase and $w_{Ph1} + w_{Ph3} = 1$ and $w_{Ph2} + w_{Ph5} = 1$. In equations (8) and (9), we do not use the multiple converted phases with negative polarity to estimate the H_2 and H_1 because their amplitudes are usually small and are often masked by other strong phases.

Using this method, we can derive H_1 (Fig. 2a) and H_2 (Fig. 2b) by locating the maximum values of S_1 and S_2. In this grid-search method, the uncertainty for the

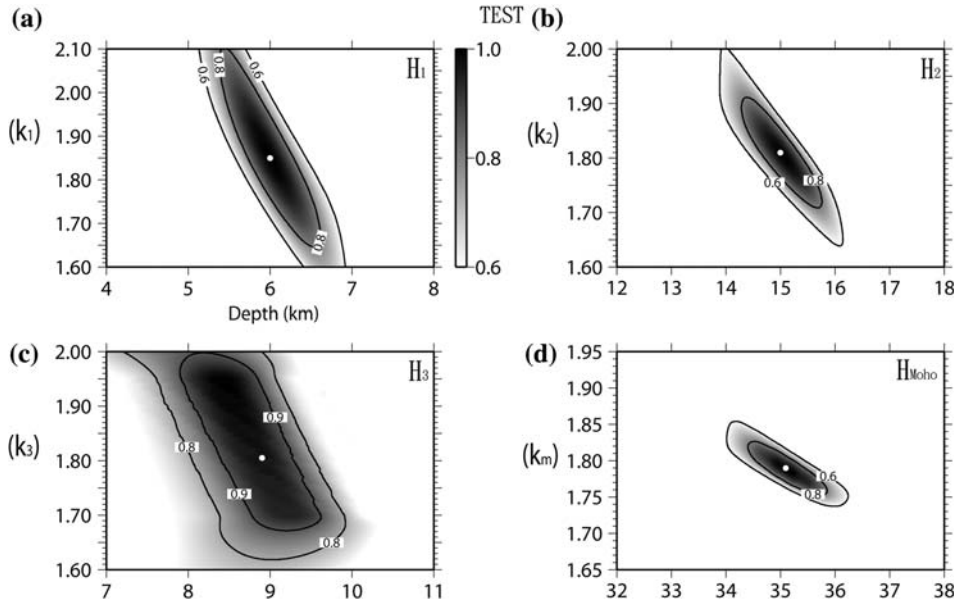

Figure 2
The stacked results are shown for **(a)** H_1, **(b)** H_2, **(c)** H_3, and **(d)** H_{Moho} with the same ray parameter of 0.065 s/km (corresponding to an epicentral distance of about 55 degree). The white spot shows the maximum of the stacked results. These results agree well with the reference model (Table 1).

discontinuity depth is smaller than that for the velocity ratio. From Figures 2a and 2b, we have arrived at reasonable H_2 and H_1 values as well as the velocity ratios.

Furthermore, the time separation between pairs among Ph3, Ph4 and Ph5 can be used to estimate H_3 from equations (10)–(12) below, again writing $1/V_{3s}^2$ into k_3^2/V_{3p}^2

$$H_3 = \frac{t_{Ph4} - t_{Ph3}}{2\sqrt{\frac{1}{V_{3p}^2} - p^2}}, \tag{10}$$

$$H_3 = \frac{t_{Ph5} - t_{Ph4}}{\sqrt{\left(\frac{k_3}{V_{3p}}\right)^2 - p^2} - \sqrt{\left(\frac{1}{V_{3p}}\right)^2 - p^2}} \tag{11}$$

$$H_3 = \frac{t_{Ph5} - t_{Ph3}}{\sqrt{\left(\frac{k_3}{V_{3p}}\right)^2 - p^2} + \sqrt{\left(\frac{1}{V_{3p}}\right)^2 - p^2}}, \tag{12}$$

where k_3 is the V_p/V_s ratio between discontinuities 1 and 2. Again, we define S_3 as

$$S_3(H_3, k_3) = w_1[r(t_{Ph4}) + r(t_{Ph3})] + w_2[r(t_{Ph5}) + r(t_{Ph4})] + w_3[r(t_{Ph5}) + r(t_{Ph3})]. \tag{13}$$

The w_i are weighting factors, and $\sum w_i = 1$. t_{Ph4} is the predicted arrival times of Ph4 and t_{Ph3} and t_{Ph5} are fixed which are obtained previously form Eqs. (8) and (9). $S_3(H_3, k_3)$

will reach a maximum when these phases are stacked coherently (Fig. 2c). The variances of H_i have the same definition used by ZHU and KANAMORI,

$$\sigma_{H_i}^2 = 2\sigma_{S_i} / \frac{\partial^2 S_i}{\partial H_i^2}, \tag{14}$$

where σ_s is the estimated variance of $S_i(H_i, k_i)$ from stacking. In our analysis, if a different P-wave velocity is used, different values of H_1, H_2, H_3 and k will result, leading to an inconsistency that the sum of H_1 and H_3 deviates significantly from H_2. Moreover, the effect of changes of P-wave velocity to the H_i (or differential times between direct P and Ps phases) is not as sensitive as to the change of the k values, as is also pointed out by ZHU and KANAMORI (2000). From the above interpretation, a more precise P-wave velocity is not necessary for more accurate results of H_i and k_i. Even though a full covariance analysis among the parameters assumed in (14) cannot be easily obtained, the additional independent check that $H_1 + H_3 = H_2$ should offer a reasonably confident estimate of the results.

3. Data Processing and Results

Data used in this study are recorded at two stations TDCB and TPUB (Fig. 3a, Table 2) of the Broadband Array in Taiwan for Seismology (BATS) for events between 2002 and 2004 with Mw $\geq$ 5.5 and epicentral distances from 30° to 65° (Fig. 3b, Table 3). These two stations are equipped with Strekeisen STS-1 (TDCB) and STS-2 (TPUB) sensors with a sampling rate of 20 sps. The two horizontal seismograms are rotated to get the radial components that are used in this study. The multiple-taper correlation (MTC) technique (PARK and LEVIN, 2000) is used to calculate the radial receiver functions (RRFs). Because this technique can obtain phases from a shallow low-velocity layer atop the crust (PARK and LEVIN, 2000; LEVIN and PARK, 1997a). To extract the important signal from the P wave coda from the raw data, a 60-s time window is used, starting 10 s before the P-arrival. The cutoff frequency (low-pass limit, 2 Hz in this study) is chosen by trial and error until we find the best RRFs profile. The weighting factors of equations (8), (9) and (13) are tested until we get optimal result with $w_{Ph1} = w_{Ph3} = w_{Ph4} = w_{Ph5} = 0.5$ and $w_1 = 0.4$, $w_2 = 0.3$, $w_3 = 0.3$.

3.1. Identifying Phases on RRF Profiles

The RRF profiles usually have seemingly disordered alignment which makes it difficult to identify each phase. For this reason, we find it logical to fix the Ph1 and Ph3 phases first as guided by each ray path (Fig. 1c), then it is easy to derive that (1) the arrival time of Ph1 must be the first; (2) Ph3 must arrive earlier than Ph4 and Ph5 must arrive as the last on a RRF profile. Accordingly, we first identify that the first major

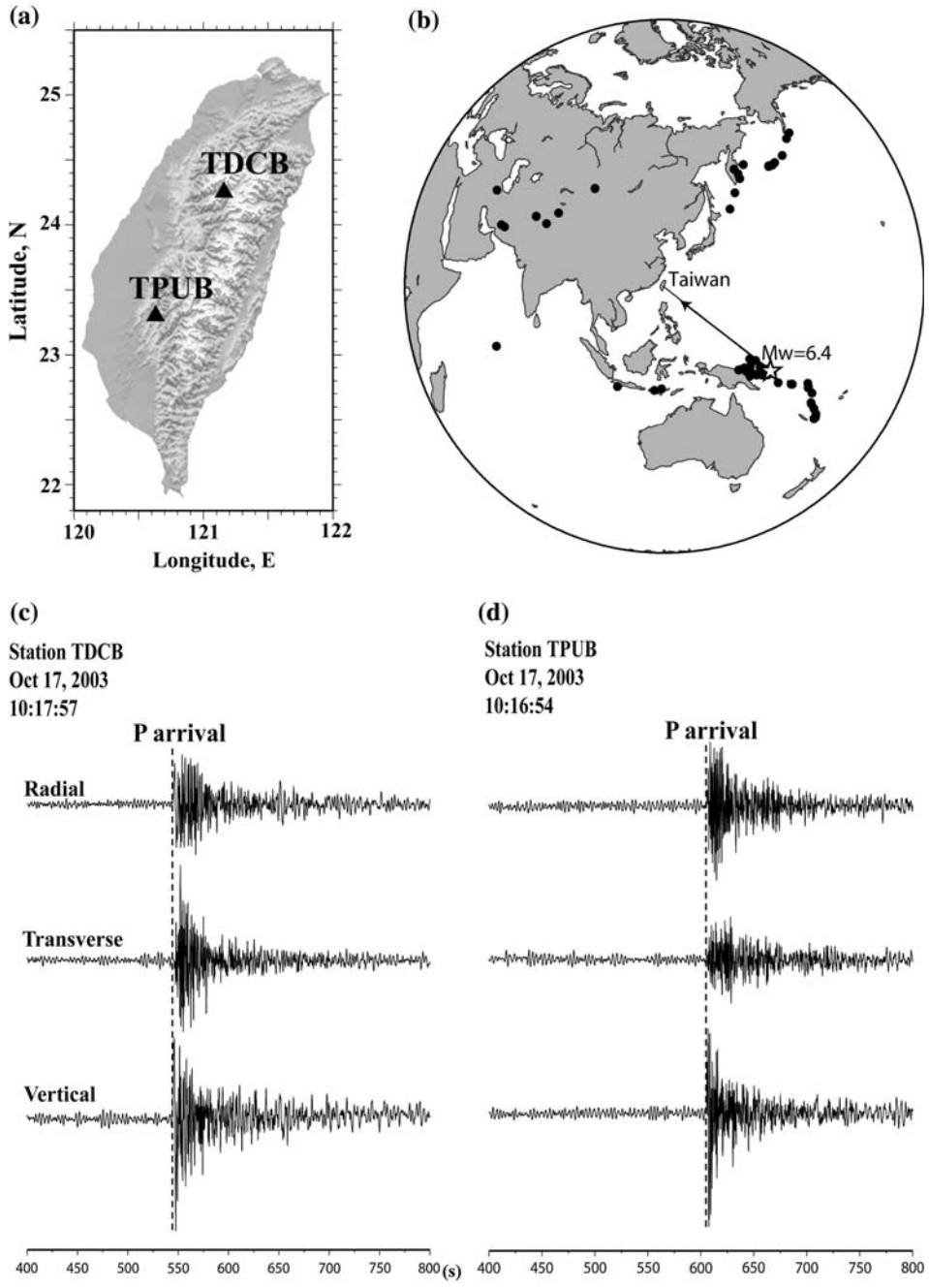
(a)
TDCB
TPUB
Latitude, N
Longitude, E
25
24
23
22
120
121
122
(b)
Taiwan
Mw=6.4
(c)
Station TDCB
Oct 17, 2003
10:17:57
P arrival
Radial
Transverse
Vertical
400 450 500 550 600 650 700 750 800 (s)
(d)
Station TPUB
Oct 17, 2003
10:16:54
P arrival
400 450 500 550 600 650 700 750 800

◀ Figure 3
(a) Location of the two stations (TDCB and TPUB) in Taiwan. **(b)** The distribution of events. The event ($M_w = 6.4$) for 10:19:06 October 17, 2003 is marked by a star located at 154.155°E and 5.471°S. **(c)** A sample of rotated seismogram recorded by station TDCB for the starred event in **(b)**. This record begins at 10:17:57 and the arrival of P wave is indicated by the dashed line. **(d)** Similar seismogram for station TPUB and this record begins at 10:16:54.

Table 2

Locations of the two stations in Taiwan under study

Station Name	Longitude, °	Latitude, °	Elevation, m
TDCB	121.1583	24.2520	1280
TPUB	120.6296	23.3005	370

phase behind the direct P wave is Ph1 on the RRF profile, we then use equations (4), (5), and (8) to find Ph3 and estimate H_1 and K_1 at the same time. After confirming Ph1 and Ph3, we search around the predicted arrival time of the Ph2 and the Ph5 on RRFs profile. From the ray path of the Ph2 and the Ph3, we cannot determine which will arrive earlier. Hence, we search these phases by trial-and-error using equations (6), (7) and (9). Of course, the results still need to satisfy the above two conditions. In our case, one phase appears between the confirmed Ph1 and Ph3 and we have identified it as Ph2. Lastly, we search Ph4 between Ph3 and Ph5 and estimate H_3 by equations (10)–(13). Ph4 is a good constraint on H_1 and H_2 as these two values must satisfy the condition: $H_1 + H_3 = H_2$.

We believe that potential users of this method do not know a priori what expected crustal structure will best fit their data when they handle a crustal RRF problem, Normally, they would first go for a gross feature by finding the Moho using the method outlined in ZHU and KANAMORI (2000). Then, if they find significant phases between Ps and P, they would use equation (8) to search for additional discontinuities as outlined in the text above, and at the same time make sure that the independent thickness check that $H_1 + H_3 = H_2$ is by-and-large satisfied.

Both BATS stations (TDCB and TPUB) are located in the western foothills region of Taiwan's main mountain range (Fig. 3a) that should have similar gross crustal structures, however it is also interesting to examine the structural differences. In order to enhance signals of the multiple crustal reflections and refractions, we stack the RRFs to average out the crustal irregularities and to improve the signal-to-noise ratio.

3.2. Finding Depth and k Value of a Layered Crust

Figures 4(a) and 5(a) show profiles of the stacked RRFs for TDCB and TPUB. The converted phases are indicated by symbols Ph1 through Ph5 with arrows pointing to their arrival times. Figures 4(b)–(e) and 5(b)–(e) show results for these two stations by

Table 3

The List of Events

Date	GMT Time	Longitude, °	Latitude, °	Depth, km	Mw
2002/12/20	14:14:42	147.943	−3.076	33.0	6.3
2002/12/12	8:30:42	153.275	−4.786	34.0	6.7
2002/12/5	11:14:30	153.435	−6.471	53.5	5.6
2002/11/26	0:48:15	−173.537	51.465	20.6	6.1
2002/11/20	21:32:30	74.515	35.414	33.0	6.0
2002/11/7	15:14:6	179.334	51.197	33.0	6.5
2002/9/24	22:54:21	161.110	−10.565	10.0	6.2
2002/9/4	14:34:15	147.769	−0.821	10.0	5.5
2002/6/29	2:39:4	166.541	−12.479	66.0	6.1
2002/6/22	2:58:21	49.022	35.589	10.0	6.4
2002/6/21	0:5:45	146.838	−4.536	33.0	5.7
2002/6/17	21:26:25	166.423	−12.658	54.5	6.7
2002/5/25	5:36:32	−161.081	53.903	33.0	6.3
2002/5/8	19:45:20	160.713	53.767	58.0	5.8
2002/4/12	4:0:28	69.350	35.986	37.0	5.9
2002/4/11	21:56:56	167.724	−14.427	10.0	6.1
2002/3/25	14:56:37	69.269	36.008	33.0	6.1
2002/3/20	14:29:58	144.978	−3.572	22.9	5.5
2002/2/28	1:50:50	151.309	−5.742	58.2	6.2
2002/2/19	0:35:45	150.980	−3.781	10.0	6.1
2002/2/5	13:27:25	151.319	−5.389	44.3	6.6
2002/1/2	17:22:53	167.853	−17.667	53.7	7.2
2003/12/27	22:38:1	169.835	−21.672	10.0	6.7
2003/12/27	16:0:59	169.766	−22.015	10.0	7.2
2003/12/26	21:26:4	169.314	−22.273	10.0	6.7
2003/12/26	1:56:52	58.311	28.995	10.0	6.5
2003/12/25	20:42:33	169.488	−22.252	10.0	6.4
2003/12/9	12:44:1	−179.272	51.334	33.0	6.1
2003/12/5	21:26:9	165.780	55.538	10.0	6.7
2003/11/25	20:19:46	150.880	−5.581	35.0	6.6
2003/11/17	6:43:6	178.650	51.146	33.0	7.7
2003/11/6	10:38:4	168.892	−19.262	113.7	6.6
2003/11/2	13:35:31	150.329	44.579	33.0	5.5
2003/10/22	11:45:30	147.727	−6.058	53.5	6.3
2003/10/17	10:19:6	154.155	−5.471	35.1	6.4
2003/10/1	1:3:25	87.721	50.211	10.0	6.7
2003/9/27	18:52:46	87.765	50.091	10.0	6.4
2003/9/22	22:59:2	153.808	−4.992	94.1	5.8
2003/8/21	4:2:9	59.773	29.053	20.2	5.9
2003/7/25	9:37:45	149.694	−1.528	24.0	6.4
2003/7/21	13:53:58	148.853	−5.481	189.6	6.3
2003/7/15	20:27:50	68.382	−2.598	10.0	7.6
2003/6/28	15:29:42	146.148	−3.325	10.0	6.2
2003/6/23	12:12:34	176.783	51.439	20.0	6.8
2003/6/16	22:8:2	159.999	55.492	174.8	6.9
2003/6/15	19:24:33	176.923	51.552	20.0	6.5
2003/6/12	8:59:20	154.758	−5.985	186.3	6.3
2003/6/7	0:32:45	152.502	−5.095	33.0	6.5
2003/5/14	7:40:36	107.315	−8.060	79.1	6.0

Table 3 Continued

Date	GMT Time	Longitude, °	Latitude, °	Depth, km	Mw
2003/5/13	21:21:14	167.744	−17.287	33.0	6.3
2003/5/4	14:54:0	166.314	−11.287	33.0	6.0
2003/4/27	16:3:40	169.773	−20.944	77.4	6.2
2003/4/24	10:56:21	154.991	48.764	43.8	6.0
2003/3/31	1:6:53	151.429	−6.183	46.8	6.1
2003/3/25	2:53:25	120.743	−8.294	33.0	6.3
2003/3/19	0:3:42	156.587	−9.388	33.5	6.1
2003/3/17	18:55:47	177.971	51.295	33.0	6.2
2003/3/17	16:36:17	177.978	51.272	33.0	7.0
2003/3/15	19:41:28	160.387	52.249	30.2	6.0
2003/3/11	7:27:32	153.238	−4.694	40.2	6.6
2003/2/24	2:3:41	77.230	39.610	11.0	6.3
2003/2/19	3:32:36	−164.643	53.645	19.0	6.6
2003/2/12	22:33:30	144.242	−3.652	10.0	6.2
2003/2/10	4:49:31	149.792	−6.011	33.0	6.2
2003/1/23	0:8:22	118.524	−8.807	33.0	5.5
2003/1/20	8:43:6	160.770	−10.491	33.0	7.2
2003/1/10	13:11:56	153.701	−5.311	71.9	6.6

an optimization process described in equations (8), (9), (13) and equation (5) of ZHU and KANAMORI (2000), respectively. From Figure 4(a), we can see some slight discrepancies of Ph3 on the stacked RRF profile. As the velocity structure beneath the Taiwan area is quite complex, the crustal interface near the receiver station may not be strictly planar, and the amplitudes of converted phases may be subject to different reflection/refraction points and incident angles due to lateral inhomogeneities. For a teleseismic ray path, small discrepancies in arrival times on the RRF profiles may also be due to the above effects near the source. We believe that ray-path distortions of the Ph3 caused by some crustal irregularities will create a broad peak in the H-k domain as plotted in Figures 4(b)–(e) and 5(b)–(e). This situation results in a slightly larger error range of the interface depth. However, by-and-large, the contour plots yield better constraints on depth than on the k value. Similar estimated results also can be seen for station TPUB.

We use equation (14) to estimate variances of the resulting H_i. By stacking a large number of events, we obtain an estimate on the data variances and combine the variances with their amplitude on RRF profiles. This finally leads to an error estimate giving the ranges of depth determination on H_1 to be 5.9 ± 0.5 km, H_2 11.7 ± 0.5 km, H_3 6.0 ± 0.8 km and Moho 30.5 ± 1.8 km for station TDCB. For station TPUB, respective values are H_1 6.5 ± 0.6 km, H_2 17.7 ± 2.1 km, H_3 10.4 ± 0.6 km and Moho 34.5 ± 2.3 km. The depths to the discontinuities H_1, H_2, and H_3 are correctly checked by the independent relation: $H_1 + H_3 = H_2$. These two BATS broadband TDCB and TPUB indeed sit on similar but clearly not identical crustal structures.

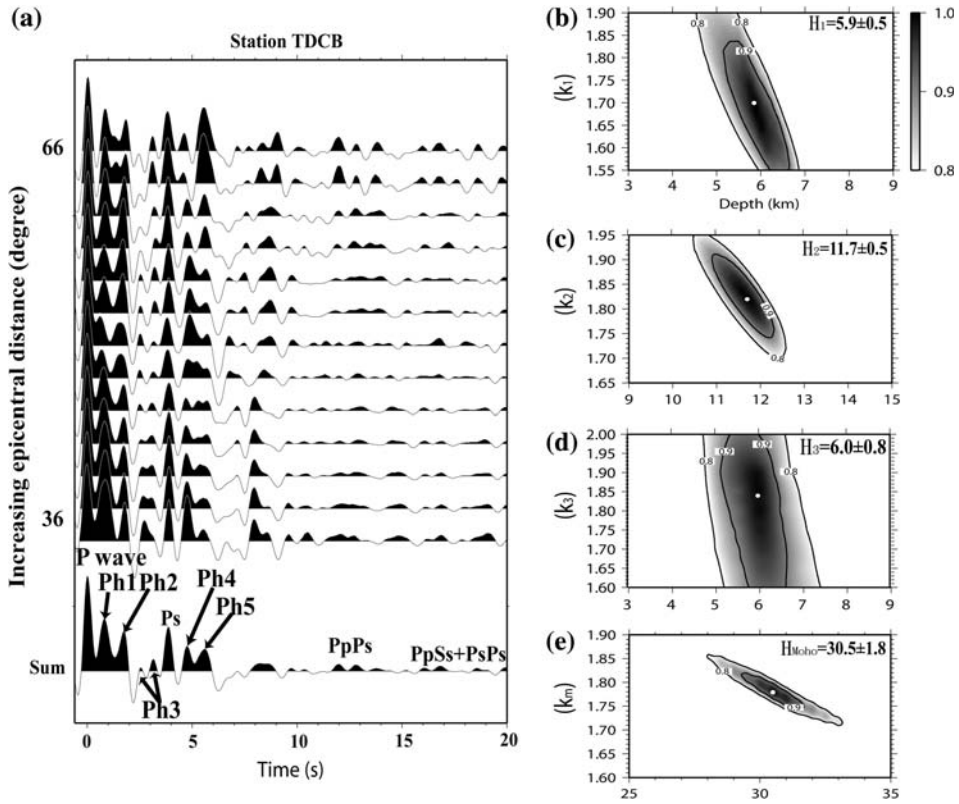

Figure 4

Estimated depths H_1, H_2, H_3, and H_{Moho} for the station TDCB with ray parameter (p) = 0.065 s/km. The white spots show the maximum of stacked results. **(a)** Results for RRF profiles and corresponding phases. **(b), (c), (d),** and **(e)** give results of stacked S function for H_1, k_1; H_2, k_2; H_3, k_3; H_{Moho} and k_m. The white spots give the maximum values of stacked results.

4. Discussion and Conclusion

In this study, we have introduced a method to extend the H-k stacking method for estimating the depths of velocity discontinuities for a three-layer crust, including the Moho depth. The extention to an N-layer case is possible to formulate, but the data resolution will not find it practical at this time. Because we ignore phases with negative polarity, we assume that there is no low-velocity zone (LVZ) in the crust. In other words, if LVZs exist in the crust, we cannot estimate accurate depths of discontinuities based on data plotted in the H-k domain alone. However from the tomographic study (i.e., RAU and WU, 1995), LVZ does not exist in the crust of Taiwan, or at least it is insignificant. Hence, our results give a reasonable crustal structure of Taiwan.

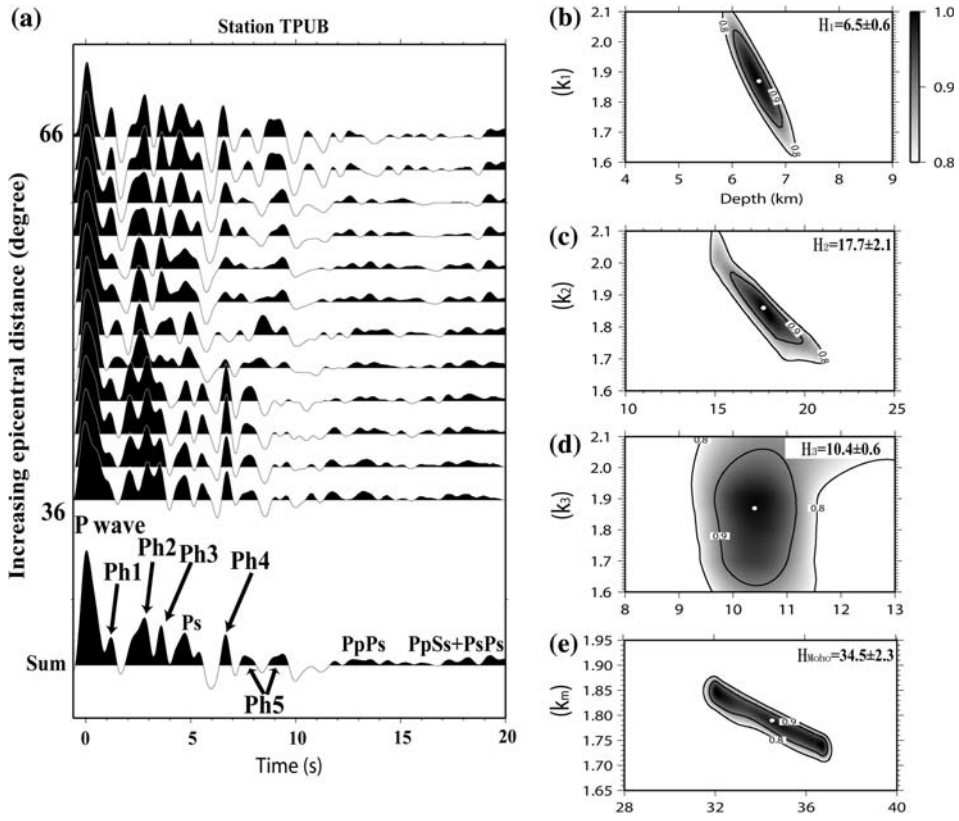

Figure 5
Estimated depths H_1, H_2, H_3, and H_{Moho} for the station TPUB with ray parameter (p) = 0.065 s/km. The white spots show the maximum of stacked S function. **(a)** Results for RRF profiles and corresponding phases. **(b), (c), (d),** and **(e)** give results for H_1, k_1; H_2, k_2; H_3, k_3; H_{Moho} and k_m. White spots show the maximum values of stacked S function.

In our method, we have stacked RRFs from teleseismic waveforms recorded by two broadband stations to enhance the signal-to-noise ratio. The robustness and stability of the method are well demonstrated. Using multiple converted phases to estimate the depths of velocity discontinuities, it is possible to obtain more detailed crustal information than using only one converted phase. However, as we have shown above, the largest uncertainty of this estimation is associated with the amplitude and arrival time discrepancies of these phases. From the event distribution, more events with epicentral distances between 35° and 45° come from a back azimuth about 130°, i.e., from the southeast. Thus our teleseismic P waves sample the crust slightly to the southeast of the stations, and RRF profiles display somewhat one-sided weighted crustal structures. However, we are still able to determine with reasonable confidence the

nature of the layered crust below those two stations, as Figures 4(b)–(e) and 5(b)–(e) show the range of layer depths (H_1, H_2, H_3 and H_{Moho}) and k values (k_1, k_2, k_3, and k_{crust}) for stations TDCB and TPUB, respectively. It is worth noting that these results check well with the independent relation $H_1 + H_3 = H_2$. The total crustal thicknesses from the two stations, both in the western foothills region of Taiwan about 100 km apart, are quite similar despite some minor variations in the depths to different mid-crust discontinuities. These discontinuities will provide a good check against results from the large-scale crustal shooting Taiger Project (under joint funding from NSF and the National Science Council of Taiwan), to take place in the Taiwan area (F. T. WU, personal communication, 2007). Also apparent in Figures 4 and 5 are that the results give better constraints on H (H_1, H_2, H_3 and H_{Moho}) than on the k values (k_1, k_2, k_3, and k_{crust}). Although the error range of k values is relatively large, the principal goal of this study is to determine H_1, H_2 and H_3, and it is accomplished reasonably well. A regional mapping of the crustal structure using this method will help clarify the tectonic development and the subsequent sedimentation/erosion history of the region. It is quite possible in this example that H_1 may be the depth to the crystalline basement upon which lay the thick Tertiary sediments in Taiwan that are actively involved in the Neogene orogeny. The H_2 is most likely the depth to the Conrad discontinuity, which is observed elsewhere in the world and by other geophysical studies in Taiwan (e.g., YEN and YEH, 1998).

Acknowledgements

This research was supported by the Taiwan Earthquake Research Center (TEC) funded through National Science Council (NSC) with grant number NSC 97-2119-M-194-011. The TEC contribution number for this article is 00035. Seismic data were obtained from the Broadband Array in Taiwan for Seismology (BATS). Many figures were prepared with the Generic Mapping Tools of *Wessel and Smith* [1991].

REFERENCES

CHEN, C.H., WANG, W.H., and YEN, Y. H. (1994), *3-D velocity structure in Taiwan: A tectonic implication of continent of continent-arc collision (abstract)*, EOS Trans. Am. Geophys. Union *75*, 645.

LEVIN, V. and PARK, J. (1997a), *Crustal anisotropy beneath the Ural Mountains foredeep from teleseismic receiver functions*, Geophys. Res. Lett. *24*, 1283–1286.

LEVIN, V. and PARK, J. (1997b), *P-SH conversions in a flat-layered medium with anisotropy of arbitrary orientation*, Geophys. J. Int. *131*, 253–266.

LEVIN, V. and PARK, J. (1998), *A P-SH conversion in layered media with hexagonally symmetric anisotropy: A cookbook*, Pure Appl. Geophys. *151*, 669–697.

LEVIN, V. and PARK, J. (2000), *Shear zones in the Proterozoic lithosphere of the Arabian Shield and the nature of the Hales discontinuity*, Tectonophys. *323*, 131–148.

LEVIN, V., PARK, J., BRANDON, M., LEES, J., PEYTON, V., GORDEEV, E. and OZEROV, A. (2002), *Crust and upper mantle of Kamchatka from teleseismic receiver functions*, Tectonophys. *358*, 233–265.

OWENS, T. J. and CROSSON, R. S. (1988), *Shallow structure effects on broadband teleseismic P waveforms*, Bull. Seismol. Soc. Am. *77*, 96–108.

PHINNEY, R. A. (1964), *Structure of the earth's crust from spectral behavior of long-period body waves*, J. Geophys. Res. *69*, 2997–3017.

PARK, J., and LEVIN, V. (2000), *Receiver functions from multiple-taper spectral correlation estimates*, Bull. Seismol. Soc. Am. *90*, 6, 1507–1520.

RAU, R.-J. and WU, F. T. (1995), *Tomographic imaging of lithospheric structures under Taiwan*, Earth and Planet. Sci. Lett. *133*, 517–532.

WU, F. W. (2007), personal communications. See also: http://www.passcal.nmt.edu/schedules/experiment_profiles/exp2006/0613TAIGER-B.html.

YEN, H.Y. and YEH, Y.H. (1998), *Two-dimensional structures of Taiwan from gravity data*, Tectonics *17*, 104–111.

ZHU, L. and KANAMORI, H. (2000), *Moho depth variation in southern California from teleseismic receiver functions*, J. Geophys. Res. *105*, 2969–2980.

(Received December 3, 2007, accepted April 25, 2008)